The United Nations University

GEOTHERMAL TRAINING PROGRAMME
Orkustofnun, Grensásvegur 9,
IS-108 Reykjavík, Iceland

Reports 1999
Number 12

INTERPRETATION OF SCHLUMBERGER AND MAGNETOTELLURIC MEASUREMENTS: EXAMPLES FROM THE PHILIPPINES AND ICELAND

Alicia N. Reyes
Department of Energy,
Energy Complex, Merritt Road,
Fort Bonifacio, Taguig,
Metro Manila,
PHILIPPINES

ABSTRACT

Geophysical studies can be a powerful tool to characterize geothermal structures at depth. Considering the rugged Philippine terrain, Schlumberger resistivity surveys are suitable for application in reconnaissance studies of geothermal prospects in terms of portability of equipment and simplicity of survey setup. Thence, characterisation of the resistivity structure at depth within resistivity anomalies defined by a Schlumberger survey can be conducted through the magnetotelluric method.

Results of the Schlumberger surveys in Cervantes geothermal prospect in Ilocos Sur, N-Philippines proved the depth limitations of direct current geophysical methods such as the Schlumberger method. However, it could be used to delineate low-resistivity anomalies in the area where future exploration efforts should be concentrated.

1. INTRODUCTION

Geophysics has proved to be a powerful tool in geothermal exploration for decades. It has been useful in delineating boundaries of geothermal systems, in characterization of the subsurface features within the geothermal field (such as resistivity, structural features, and intrusive bodies), and in siting favourable drillhole locations. Several geophysical methods are available, depending on the purpose and intent of the geophysical study, but for geothermal exploration, the most widely applied and found to be most useful, is the resistivity method. The reason for its preference is the direct relationship of resistivity to subsurface parameters that are of specific geothermal interest such as temperature, salinity, porosity (water content), permeability and hydrothermal alteration. These parameters determine the resistivity signature of an area and a geothermal area is defined as a low-resistivity anomaly.

There are two types of resistivity methods: the direct current (DC) and the electro-magnetic (EM) methods. The DC resistivity method has been largely used for reconnaissance studies of geothermal fields. DC methods are used to define near surface features such as upflow zones and vertical structures (head-on profiling method) and to delineate low-resistivity zones in the uppermost kilometre, using for

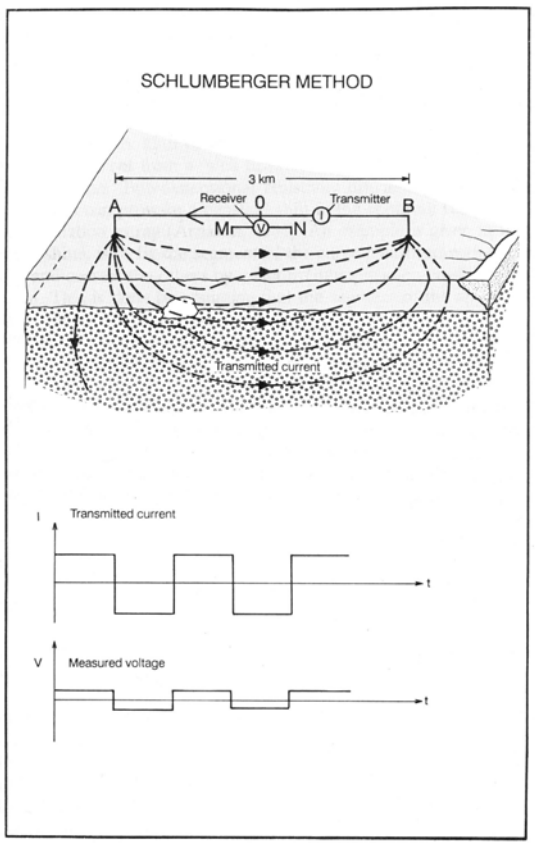

FIGURE 1: The Schlumberger setup (Hersir and Björnsson, 1991)

example the Schlumberger configuration (Figure 1). The EM resistivity methods are electromagnetic surveys that include transient electromagnetics (TEM) and magnetotelluric (MT) methods. The TEM soundings have a more downward focussing and a better depth penetration than the Schlumberger survey (up to 1.5 km) and their operation and interpretation are relatively simpler. Conducting a TEM survey is fast and requires less manpower. The one-dimensional interpretation of TEM soundings yields comparable results to the two-dimensional interpretation of Schlumberger soundings. The TEM method has a good resolution at depth and, based on Icelandic experience, it has been used successfully in delineating and identifying high-temperature fields and identifying water bearing layers in low-temperature areas. The MT method, on the other hand, probes deeper into the subsurface at depths of tens of kilometres and is, therefore, preferred for detailed geophysical survey and in exploration of deep seated geothermal systems and crustal studies.

Recent inventory of the Philippine geothermal resources identified several new prospects, mostly of low-temperature character. The inventory carried out reconnaissance of geological and geochemical surveys in the areas and the Government plans to initiate exploration work (such as geophysics) in these areas inasmuch as investors interests are still focussed on exploration and exploitation of high-temperature geothermal fields. The geophysical study will further characterize these green fields and, thus, help promote the low-temperature fields and effectively reduce the risk of their prospective developers. Considering availability of geophysical equipment, purpose of survey and applicability to Philippine terrain, the author chose to do resistivity and magnetotelluric interpretations for this project paper. In late 1997, the Department of Energy (DOE) conducted jointly with COMEXCO, Inc. (1988) through contract agreement, an integrated geoscientific study over the Cervantes geothermal prospect in Ilocos Sur, N-Philippines to determine possible application of the geothermal resource. The study included a resistivity survey consisting of the Schlumberger Resistivity Traverse (SRT) and Vertical Electrical Sounding (VES). Data acquired from the surveys were used in the Schlumberger resistivity interpretation while a sample of magnetotelluric data from a geothermal field in Central Iceland was used for the exercise on one-dimensional inversion of magnetotelluric soundings.

The project serves to strengthen the capability of the author in geophysical interpretation. Further, this paper fulfills the requirements of the UNU Geothermal Training Programme which the author underwent in April-October in 1999 at Orkustofnun, Reykjavik, Iceland.

2. THE SCHLUMBERGER RESISTIVITY METHOD

2.1 Methodology and instrumentation

The electrodes through which current is introduced into the ground are iron bars hammered into the ground. The bars are connected by insulated cables to a generator. The cables are checked for leaks to ensure the current enters or exits the ground only at the two current electrodes. For the potential

electrodes, ceramic vessels filled with saturated solution of copper sulphate kept in contact with a copper wire, are used. To ensure saturation, undissolved crystals of copper sulphate remain in the solution. The current electrodes are disposed outermost and the potential electrodes in between the current electrodes (Figure 2).

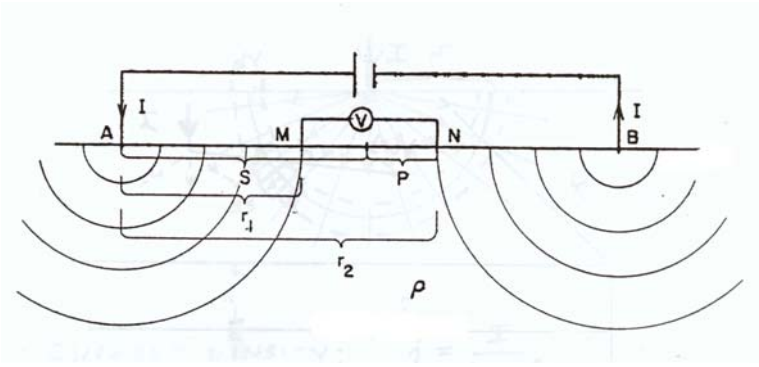

FIGURE 2: The Schlumberger configuration showing current (AB) and potential (MN) electrode spacings

For the resistivity traverse (SRT), the current electrode spacing (AB/2) distances used is usually 250 and 500 m. The potential electrode spacing (MN) is kept constant at 25 m. In the resistivity survey carried out at the Cervantes geothermal prospect in the Philippines, the current source was a portable battery powered resistivitymeter that can introduce 0.75 amps of current into the ground. The Hewlett Packard Micro Voltmeter Model 419A, equipped with a voltage biasing unit to filter natural noise, registered the voltage difference. A total of 43 SRT stations were measured.

For a sounding, the position of the current electrodes is moved outwards by the same distance from the centre of the profile to increase the depth of penetration of the sounding (the depth of penetration being equal to AB/2). The AB/2 distance is varied from 10 to 1250 m. There are instances when the MN distance has to be increased to ensure a potential difference large enough to be measured with accuracy and so MN spacing is gradually increased from 1 to 160 m. Overlap measurements are taken with every change in MN spacing. The current transmitter used in the resistivity survey carried out at the Cervantes geothermal prospect in the Philippines, was a portable Phoenix Induced Polarization Transmitter Model 1PT 1C which delivers a current of up to 5 amps at a frequency of 0.1 Hz. This transmitter was connected to a portable Honda G200 generator. The Phoenix resistivity receiver Model RV2 measures voltage difference at 4 stacks.

VES measurements are plotted on a log-log paper (apparent resistivity vs. AB/2) in the field to determine bad data and thereby facilitate repeat measurements in real time.

2.2 Theoretical background

The basic principle of resistivity surveys is to induce electrical currents in the ground and monitor signals generated by the current distribution at the surface (Hersir and Björnsson, 1991). The study deals mainly with how current flows in the rocks. The basic relationship to explain this is Ohm's Law which states that:

$$E = \rho j \quad (1)$$

where E = Electrical field intensity;
ρ = Resistivity of a homogenous earth;
j = Density of current flowing through the rock.

In terms of potential difference, which is the one measured at the surface in response to current induction in the ground, Ohm's Law is written as:

$$\Delta V = \rho I \quad (2)$$

where ΔV = Potential difference;
I = Electric current.

Considering a point source and a homogenous earth, the potential field must have cylindrical symmetry with respect to the vertical line through the current source such that:

$$V_{(r)} = \frac{\rho I}{2\pi r} \tag{3}$$

where r = Distance from the point source to where potential is measured (refer to Figure 2).

The potential difference is measured between points M and N, therefore, the potential difference can be stated as:

$$\Delta V = V_M - V_N = \frac{\rho I}{2\pi} 2\left(\frac{1}{r_1} - \frac{1}{r_2}\right) = \frac{\rho I}{K} \tag{4}$$

Computing for the resistivity, Equation 4 becomes

$$\rho = \frac{\Delta V}{I} K \tag{5}$$

where K = The geometric factor, defined as

$$K = \pi \frac{1}{\left(\frac{1}{r_1} - \frac{1}{r_2}\right)} \tag{6}$$

But, $r_1 = S - P$ and $r_2 = S+P$. Therefore, restating K in terms of S and P, Equation 6 becomes

$$K = \pi \frac{S^2 - P^2}{2P} \tag{7}$$

where S = Half of the current electrode spacing (AB/2);
P = Half of the potential electrode spacing (MN/2).

Equation 5 is derived for a theoretical homogenous earth. In realistic sense, the subsurface is not homogenous and, therefore, the resistivity value obtained should be termed only as an "apparent resistivity" such that the equation shall be written as:

$$\rho_{app} = \frac{\Delta V}{I} K \tag{8}$$

Adapting the solution for the differential equation of Laplace and considering the conditions set for a horizontally stratified earth, we arrive at the equation for the potential (Koefoed, 1979, p.27-29):

$$V_i = \frac{\rho_i I}{2\pi} \int_0^\infty K(\lambda) J_o(\lambda r) d\lambda \tag{9}$$

where K = The Kernel function;
J_O = The Bessel function of zero order;
V_i = Potential at surface point;
ρ_i = Resistivity of the first layer;
r = Distance from the current source to the voltage measuring point.

Using gradient approximation, where S is increased such that P is infinitesimally small compared to S, the equation, where the apparent resistivity is a function only of the current injected, I, and the electrode spacing, S, is reduced as follows (Koefoed, 1979):

$$\rho_a(r) = r \int_0^\infty K(\lambda) J_1(\lambda r) \lambda \, d\lambda \tag{10}$$

2.3 Modelling programs

Three programs were used in the processing of the Schlumberger sounding measurements in order to come up with models indicating how many layers of earth with different resistivities occur at depth and how thick each of these layers is. The programs are PSLINV, SLINV and SPLOT.

PSLINV facilitates input of data from the keyboard or reading of data from an existing file, then prepares the data for SLINV processing.

SLINV is a one-dimensional nonlinear, least-squares inversion program for Schlumberger resistivity soundings, after the Levenberg-Marquardt inversion algorithm. The program is nonlinear as the data and model parameter inputs are processed in logarithmic form to downplay non-linearity in the dependence of the resistivity on the model parameters. The main task of the program is to iteratively adjust the free model parameters until the model curve approximates the measured apparent resistivity curve. The iteration does not change the number of layers assumed in the model parameters so trials on different layering have to be performed to determine the best model. The quality of the fit is measured by the CHI value. The rule is, the lower the CHI value, the better the fit. The forward algorithm used in the program to calculate the apparent resistivity values for a given one-dimensional model applies gradient approximation where the potential electrode spacing MN is made very small compared to the current electrode spacing AB. The reason for this is to make the apparent resistivity a function of AB/2. The algorithm calculates the apparent resistivity values for the given model. The results of the modelling are captured in a list file for the numerical values of the iterations, and a plot file which facilitates presentation of the results in double logarithmic graphical form.

SPLOT utilizes the plot file generated by SLINV to present the graph of the measured vs. calculated apparent resistivities, the model's numerical values in terms of resistivity and thickness of the layers, and the histogram of the model plotted as resistivity vs. depth. The measure of the fit is indicated in the plot as CHI value. The sounding station identification indicated is based on the name of the plot file.

2.4 Resistivity of rocks

Rocks are inherently nonconductive and therefore, generally, of high resistivity to current flow. The conductivity in the rock is mainly due to water contained in its pores or to solutions flowing through it or due to conductive alteration minerals. Geothermal areas are water-saturated areas and in effect, geothermal exploration is particularly concerned with low-resistivity (or conductive) signatures. In interpreting the resistivities, the understanding of the factors responsible for the resistivities and the factors affecting the trend of the measured parameters are indispensable. Relationships presented here are taken from Hersir and Björnsson (1991). Original references for the equations are found therein.

Resistivity as a function of salinity and mobility of ions. Conductivity of solutions is largely a function of salinity and the mobility of the ions present in the solution is expressed in the equation:

$$\sigma = \frac{1}{\rho} = F \times (c_1 q_1 m_1 + c_2 q_2 m_2 + ...) \qquad (11)$$

where σ = Conductivity;
F = Faraday s number [96,500 coulombs];
c = Concentration of ions;
q = Valence of ions;
m = Mobility of ions.

Resistivity as a function of temperature. From Equation 11, it can be seen that the resistivity has an inverse relationship with salinity (in terms of concentration of ions) and mobility of the ions. Ion mobility is a function of temperature and viscosity such that the relationship of resistivity to temperature can be approximated by the following relationship:

$$\rho_w = \frac{\rho_{wo}}{1+\alpha(T-T_o)} \tag{12}$$

where ρ_{wo} = Resistivity of fluid at temperature T_o (Ωm);
α = Temperature coefficient of resistivity, which can be approximated as $0.023^{\circ}C^{-1}$ for $T_o = 23^{\circ}C$ and $0.025^{\circ}C^{-1}$ for $T_o = 0^{\circ}C$.

Resistivity as a function of porosity and permeability. Since the fluid is often important for the conduction in the rock, then, the degree of saturation is of importance to the bulk resistivity (Hersir and Björnsson, 1991). According to Archie s law, resistivity of water-saturated rocks varies approximately as the inverse square of the porosity (at pore fluid resistivity $\rho_{wo} \leq 2$ Ωm).

$$\rho = \rho_w a \phi_t^{-n} \tag{13}$$

where ρ = Bulk resistivity;
ρ_w = Resistivity of the pore fluid;
ϕ_t = Porosity;
a = Empirical parameter for describing type of porosity, usually ~1;
n = Cementing factor, usually ~ 2.

The amount of fluid flowing through the rock can also be largely dictated by the secondary permeability provided by fractures, especially in geothermal areas. The wider the fractures, the higher is the fracture porosity, thence, high permeability according to the equation:

$$k = \frac{d^3}{12F} \tag{14}$$

where k = Permeability;
d = Mean fracture width;
F = Mean distance between fractures.

Resistivity as a function of fluid-rock interaction. Aside from resistivity of the pore fluid, bulk resistivity of the rock is also reduced by the presence of hydrous secondary minerals (i.e. clays) as products of fluid-rock interaction expressed in terms of interface conductivity (alteration). This can be illustrated by the equation:

$$\sigma = \frac{1}{F}\sigma_w + \sigma_s \tag{15}$$

where σ = Bulk conductivity;
σ_w = Conductivity of water;
σ_s = Interface conductiviy;
F = Formation factor.

2.5 Factors affecting apparent resistivity curves

2.5.1 Subsurface resistivity contrast

Strongly differing layer distributions in the subsurface may yield apparent resistivity curves that, although not strictly equal, differ so slightly that they cannot be separately distinguished within the accuracy of the measurements (Koefoed, 1979). The phenomena can either be an “equivalence” or a “suppression”. There are two types of equivalences. In both cases, there is a layer whose thickness and resistivity is undetermined. For both cases, the depth to this layer’s interface must be the same or less than the thickness of this undetermined layer. The first one is a bell type curve, i.e. a resistive layer which is

embedded between two conductive layers. In this case, the only known parameter for the intermediate layer is the transversal resistance, given by the product, $\rho_i d_i = T$. The second one is a bowl type curve, i.e. a conductive layer which is embedded between two resistive layers. In this case, the only known parameter for the intermediate layer is the longitudinal conductance, given by the only known parameter for the intermediate layer is the longitudinal conductance, given by the quotient $d_i/\rho_i = S_L$. In the presence of equivalence layers in one-dimensional interpretation, it is advisable to add some independent information from other investigations. If they are not available, correlations can be made utilizing other soundings in the neighbourhood (Hersir and Björnsson, 1991).

Suppression is when resistivity of the layers increases with depth (ascending type sequence) or decreases with depth (descending-type). In the ascending and descending-type sequences (Figure 3), the effect is such that it may be impossible to detect the existence of the intermediate layer at all from the resistivity curve.

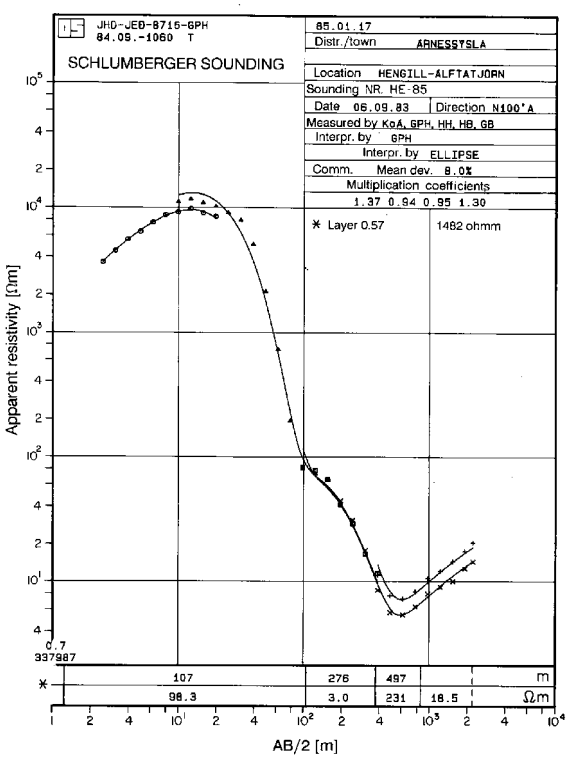

FIGURE 3: One-dimensional interpretation of a Schlumberger sounding from Hengill, SW Iceland showing equivalent layers and types of shifts in apparent resistivity curves (Hersir and Björnsson)

2.5.2 Inhomogeneities

In contrast to the initial assumptions of homogeneity for the earth layers, geological formations are generally not isotropic. The anisotropism is such that there is higher resistivity perpendicular to the stratification (transversal resistance) than along the stratification (longitudinal conductance). The situation applies in one case where there is electrical anisotropy within one layer (such as in clays and shales). Another case, called pseudoanisotropy, concerns alternating facies made up of thin beds. The anisotropy cannot be detected by the sounding measurements but its practical effect, if its occurrence is not known from other sources, is that too large values will be obtained for the thicknesses of the anisotropic layers (Koefoed, 1979).

Continuous changes of resistivity or conductivity with depth is also a case that should also be looked into in interpretation. An example of this is when there is continuous increase of resistivity with depth reflecting weathering of a pluton at the surface and its gradual transition to fresher conditions at depth. The trend is not reflected in the sounding measurements so clearly that the changes can be reflected as intermediate separate layers.

2.5.3 Shifts

There are instances in the conduct of resistivity surveys when the potential electrode spacing has to be changed to improve the signal strength in the resistivity measurements with increased current electrode spacing. In such cases, you get overlapping segments in the apparent resistivity curves and these segments often do not tie-in with the general trend of the curve and these are termed ‘shifts’.

There are two types of shifts: the convergent shift and the constant shift (Figure 3). The convergent shift eventually ties in at larger AB/2 distances by gradient approximation. This shift is mainly due to large resistivity contrasts between layers in the stratified earth. The constant shift does not tie in at all and the deviation from the main curve remains throughout all the set of measurements. This particular case is due to the presence of a local lateral inhomogeneity near the potential electrodes. As a solution, the potential electrode station should not be located in an area suspected to be of less resistivity than the environment, or regarding the model, the readings with the largest potential electrode spacing are considered as close to the true resistivity, for it may have already avoided the interference of the local inhomogeneity (Árnason, 1984).

3. RESISTIVITY SURVEY OF THE CERVANTES GEOTHERMAL PROSPECT

Cervantes geothermal prospect is located in Ilocos Sur, north of Luzon Island, Philippines (Figure 4). It is bounded on the north by Abra Province, on the west by the rest of Ilocos Sur, on the east by Mt. Province and Ifugao Province and on the south by Benguet Province. Resistivity surveys comprising of the Schlumberger resistivity traverse (SRT) and the vertical electrical sounding (VES) were conducted in the area on October 18-November 26, 1997 to delineate low-resistivity anomalies which might indicate boundaries of a geothermal reservoir underneath.

The 320 km^2 surveyed area lies along a graben valley where Cervantes municipal proper is located. The area is flanked by cordilleras on both sides and drained by the wide and long Abra River. Upstream, part of Abra river is in the vicinity of Mankayan, draining down to Quirino in the north. There were 9 VES stations and 43 SRT stations included in the survey (Tables 1 and 2 and Figure 5).

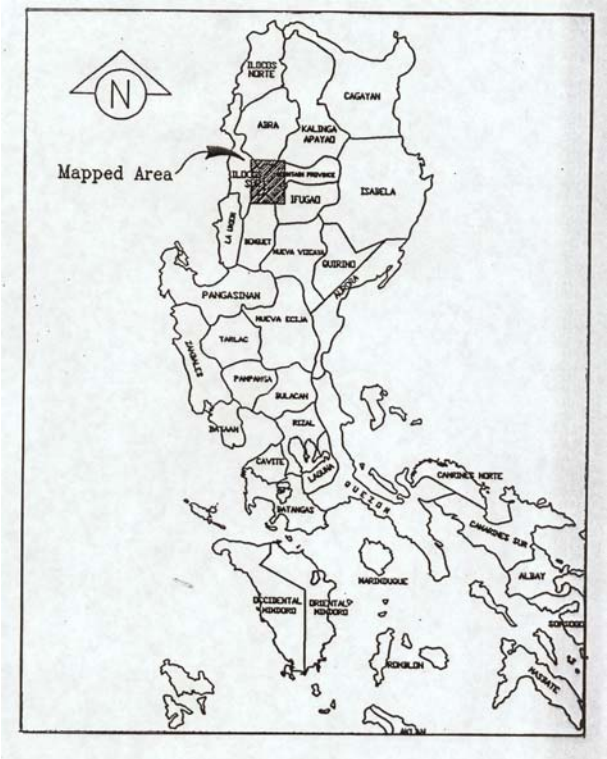

FIGURE 4: Location Map of Cervantes geothermal prospect (Comexco, 1998)

TABLE 1: Coordinates and elevation of vertical electrical sounding stations (VES)

VES station no.	Coordinates		Elevation (m a.s.l.)
	Northing	Easting	
1	16°57.60'	120°44.82'	565
2	17°01.66'	120°42.92'	710
3	17°05.66'	120°42.02'	710
4	16°56.75'	120°48.62'	935
5	16°56.20'	120°44.64'	575
6	16°58.54'	120°39.45'	1445
7	17°00.24'	120°47.68'	1200
8	16°54.08'	120°46.12'	870
9	16°58.88'	120°43.38'	515

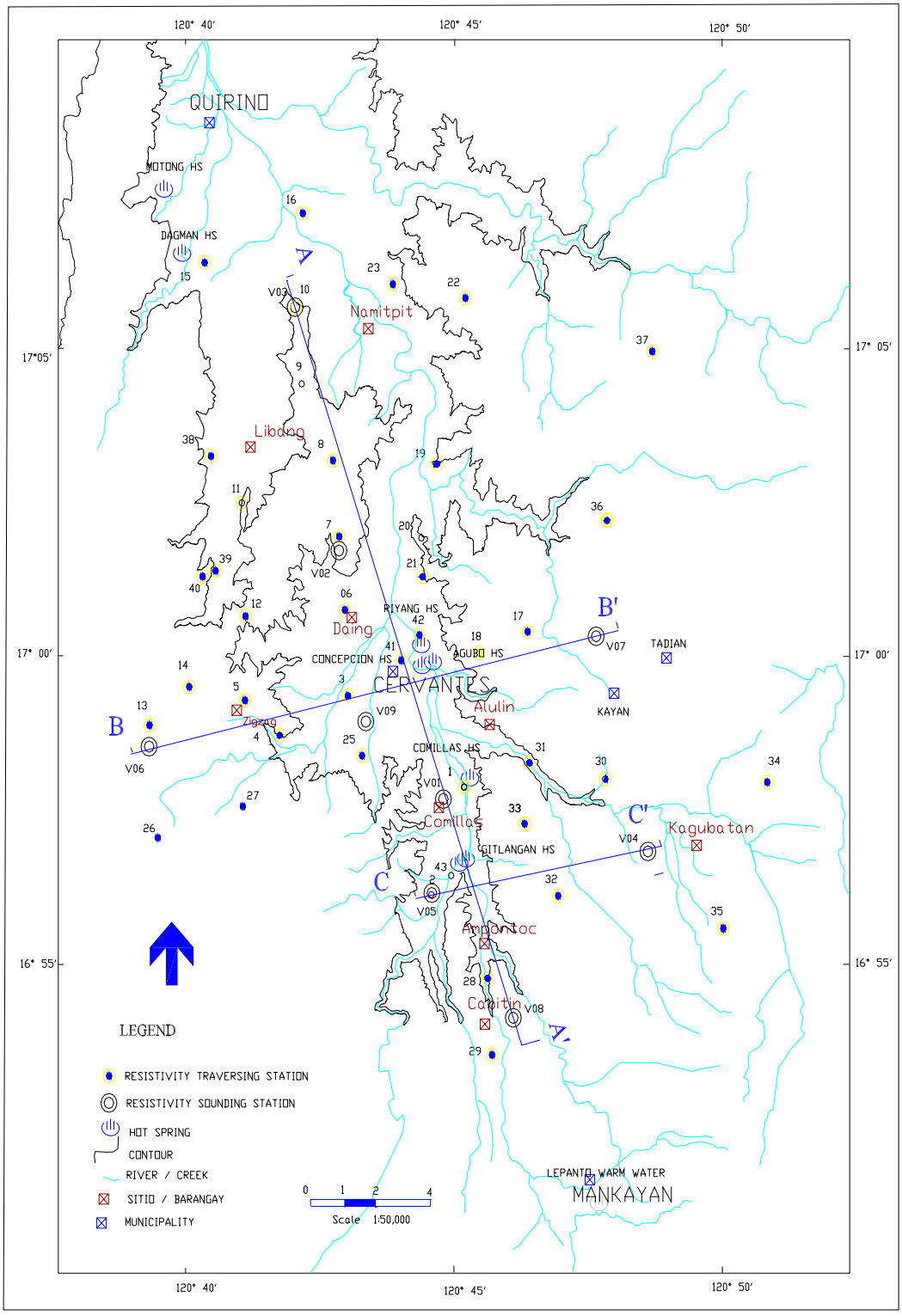

FIGURE 5: Location map of the resistivity survey stations in Cervantes geothermal prospect (modified from Comexco, 1998)

TABLE 2: Coordinates and elevation of Schlumberger resistivity traverse stations (SRT)

SRT station no.	Coordinates		Elevation (m a.s.l.)	SRT station no.	Coordinates		Elevation (m a.s.l.)
	Northing	Easting			Northing	Easting	
1	16°52.88'	120°44.80'	500	23	17°06.06'	120°43.90'	500
2	16°56.20'	120°44.64'	500	24	16°57.30'	120°43.66'	600
3	16°59.36'	120°43.05'	500	25	16°58.38'	120°43.32'	500
4	16°58.70'	120°41.78'	600	26	16°57.09'	120°39.54'	1800
5	16°59.28'	120°41.12'	700	27	16°57.62'	120°41.06'	1300
6	17°00.72'	120°42.98'	500	28	16°54.78'	120°45.65'	600
7	17°01.89'	120°42.90'	600	29	16°53.54'	120°45.74'	800
8	17°03.18'	120°42.78'	800	30	16°58.00'	120°47.86'	600
9	17°04.32'	120°42.30'	700	31	16°58.26'	120°46.46'	500
10	17°05.60'	120°42.02'	650	32	16°55.10'	120°46.96'	900
11	17°02.44'	120°41.06'	600	33	16°57.25'	120°46.35'	700
12	17°00.64'	120°41.12'	600	34	16°57.95'	120°50.92'	1100
13	16°58.92'	120°38.40'	1400	35	16°55.55'	120°50.05'	1300
14	16°59.54'	120°40.12'	900	36	17°02.22'	120°47.88'	1100
15	17°06.40'	120°40.28'	500	37	17°04.96'	120°48.74'	1400
16	17°07.14'	120°42.30'	400	38	17°03.24'	120°40.30'	500
17	17°00.38'	120°46.40'	800	39	17°01.38'	120°40.58'	500
18	17°00.02'	120°45.52'	800	40	17°01.30'	120°40.32'	600
19	17°03.14'	120°44.70'	600	41	16°59.92'	120°44.05'	500
20	17°02.16'	120°44.30'	600	42	17°00.34'	120°44.36'	500
21	17°01.28'	120°44.44'	600	43	16°56.62'	120°45.08'	500
22	17°05.80'	120°45.24'	900				

3.1 Geology

The area is underlain by eight rock types with age ranging from Pre-Eocene to Recent (Table 3 and Figure 6). The cordilleras flanking the valley consist of the basement complex which is the oldest rock type found within the prospect. The basement complex is composed of basalt and andesite flows moderately altered by epidote and chlorite by regional metamorphism. The depression itself is dominated by Early to Late Miocene laharic flows of dacite, andesite tuff breccias and pyroclastics intercalated with sandstone, siltstone and conglomerate. Recent sediments are deposited in the immediate vicinity of the river.

Down south from Comillas towards Mankayan, intrusions of medium-coarse-grained quartz diorite/granodiorite were mapped. These intrusions are believed responsible for the mineralizations noted in the area. The western extremity at the north of the surveyed area and the eastern extremity at the south along Kagubatan area are exposures of the Balili formation. The formation consists of andesitic volcaniclastics and sedimentary sequences of Late Eocene to Early Miocene age.

Fault structures trend northwest at the southern half of the prospect area shifting to a north-south trend towards Quirino. The dominant structure is the wrench fault named Abra river fault (Comexco, 1998) truncating the cordillera at the west. It has a major splay, the east Abra river fault, the trace of which is defined by the course of the main Abra river. These major faults define the western and eastern boundaries of the valley mapped.

There are seven hot spring areas in the region, from north to south of the mapped area: Motong, Dagman,

Riyang, Agubo, Concepcion, Comillas and Gitlangan. The hot springs are located along the trace of the faults. Geochemical estimates by COMEXCO (1998) indicate possible reservoir temperature of 90-120°C with the probable heat source in Mankayan.

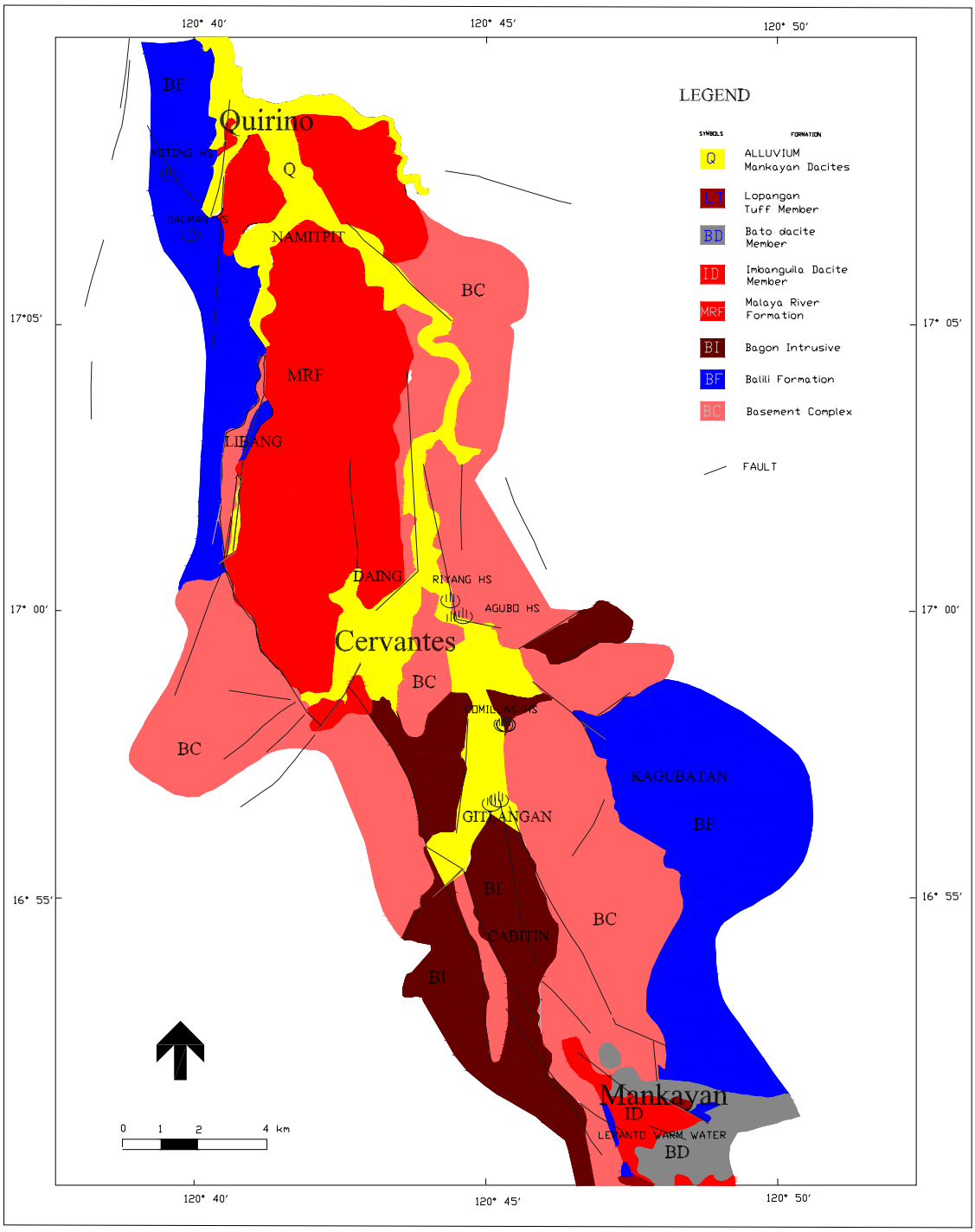

FIGURE 6: Geologic map of Cervantes geothermal prospect (Modified from COMEXCO, 1998)

TABLE 3: Stratigraphic column in the Cervantes geothermal prospect area (Comexco, 1998)

Formation	Age	Description
Alluvium	Recent	River deposits
Mankayan dacites		
Lapangan tuff	Late Pleistocene	Dacite tuff
Bato dacite	Late Pliocene to Early Pleistocene	Dacite porphyries and pyroclastics
Imbanguila dacite	Late Miocene to Early Pliocene	Dacite porphyries and pyroclastics, generally altered
Malaya river formation	Late Miocene to Early Pliocene	Dacite/andesite tuff breccias, pyroclastic flows inter-calated with sandstone, siltstone and conglomerate
Bagon intrusive	Early Miocene	Medium- to coarse-grained quartz diorite or granodiorite
Balili formation	Late Eocene to Middle Miocene	Volcaniclastics, tuff breccias, sandstone, shales, limestone and conglomerates
Basement complex	Pre-Late Eocene	Partly metamorphosed basalt and andesite flows/breccias

3.2 Discussion of results

3.2.1 The Schlumberger resistivity traverse measurements

The measurements acquired from the resistivity traverse covering 43 stations (Figure 5) were mapped, and iso-resistivity lines were constructed to determine low-resistivity anomalies. Separate iso-resistivity contours were made for AB/2 = 250 m (Figure 7) and AB/2 = 500 m Figure 8). The iso-resistivity maps do not lie on a plane but were constructed from the surface. The contours for both current electrode spacings revealed two low-resistivity anomalies defined by the 50 Ωm iso-resistivity line. The first anomaly is located at Cervantes extending northwards to Namitpit area. This anomaly opens up to Quirino. The anomaly is elongated and the trend is north-south. It coincides with the trace of the Malaya river formation which is composed of dacite/andesite tuff breccias and pyroclastic flows, and intercalations of sandstone, siltstone and conglomerate. This formation is highly porous and in places, moderately to intensely altered by

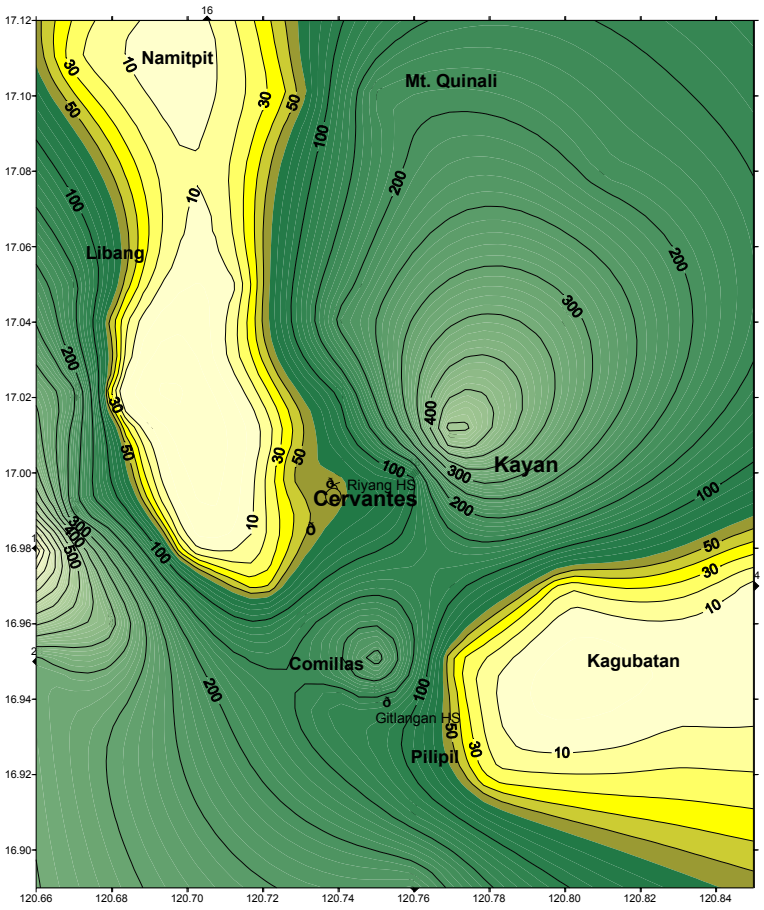

FIGURE 7: Cervantes geothermal prospect, iso-resistivity map for AB/2 = 250 m

clay and goethite/hematite. Most of the resistivity readings within the anomaly are of the order of 10 Ωm. The hot springs found in Namitpit are located just at the foot of the western cordillera and are peripheral to the low-resistivity anomaly.

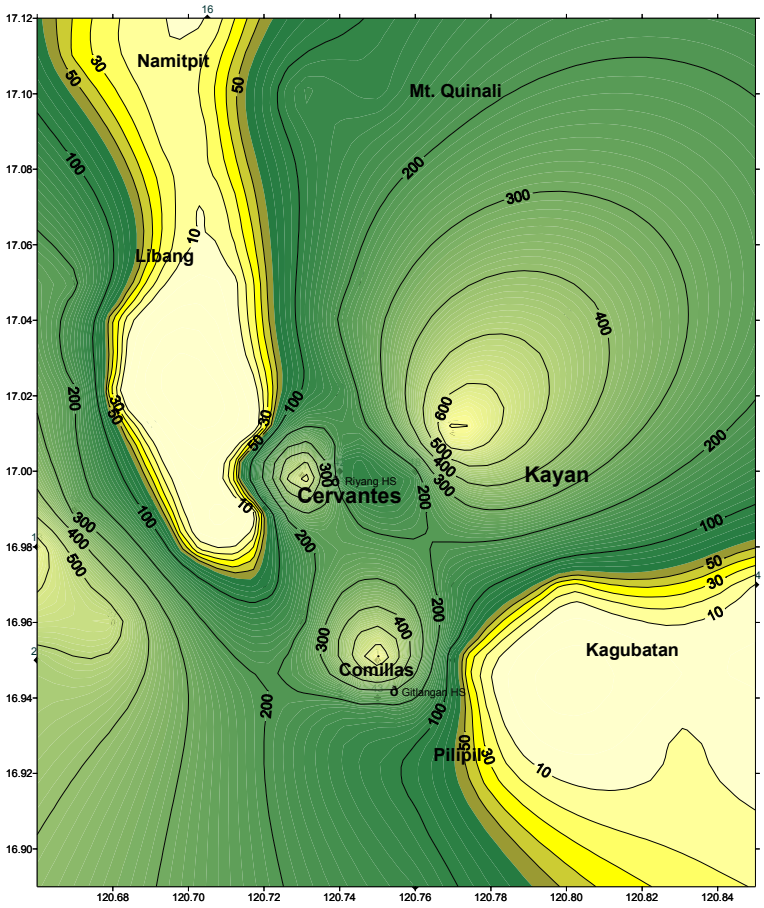

FIGURE 8: Cervantes geothermal prospect, iso-resistivity map for AB/2 = 500 m

The second anomaly lies around Mt. Kagubatan. The anomaly is twice as broad as the Namitpit anomaly. Resistivity measurements within the anomaly are at around 20 Ωm in the west down to around 10 Ωm towards the east. Like the Namitpit anomaly, the Kagubatan anomaly is located within the Balili Formation which is composed of volcaniclastics, tuff breccias and sedimentary units such as shales, wackes and conglomerates. Whereas, the Namitpit volcaniclastics are dacitic in composition, the Kagubatan formation consists of andesitic to basaltic volcaniclastics. The alteration is mainly chlorite and epidote plus some veinlets of zeolite and quartz. The center of the anomaly is a remnant two-pyroxene basalt volcanic neck. It is difficult to determine the factors responsible for the low resistivity in Kagubatan. Only one station is located in the area and very little mapping has been done in the vicinity because the site is already out of the boundaries defined in the contract-out survey agreement with COMEXCO. The anomaly is therefore not well constrained.

The high resistivity areas plot and coincide with the cordilleras bounding the valley where the low-resistivity anomalies are located, particularly the Bessang Pass to the west and Mt. Quinali and Mt. Arno in Kayan to the east. These cordilleras constitute the metamorphosed basement complex which is slightly to moderately altered by chlorite and epidote.

The trend of the Namitpit resistivity anomaly narrowed a bit at deeper levels as shown by iso-resistivity contours at AB/2 = 500 m. At the same level, the Kagubatan anomaly seems to have spread south of the municipality of Pilipil. This may not be surprising as there is a copper mine in that direction and a hot spring is actually present at level 700 of the mine.

From the iso-resistivity maps, it seems that the two anomalies are separate and distinct as high resistivities register in-between them. These high resistivity patches may be tongues of the intrusive rocks which are relatively less altered than the surrounding volcaniclastics. Further conclusions shall be deduced in the interpretation of the soundings which probed at depth.

3.2.2 The vertical electrical soundings

To probe the resistivities at more depth within the anomalies defined by the SRT, VES measurements were taken at the Daing-Namitpit area (V2, V3 and V9) all the way through to Cabitin (V1, V5 and V8),

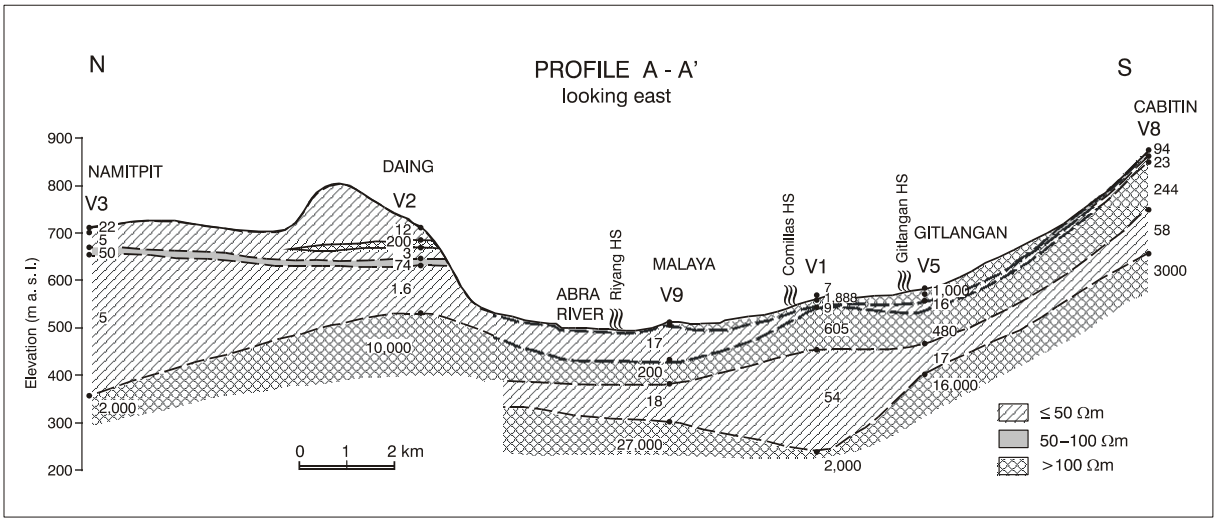

FIGURE 9: Resistivity cross-section A-A'

and at the Kagubatan area (V4). Measurements were also taken at Bessang Pass and Kayan to confirm the high resistivities revealed by SRT in these areas (Figures 7 and 8).

Profiles from the layer models of the VES soundings show layers of high and low-apparent resistivity in the upper 400 m from the surface. The layering is depicted at lower elevation where the VES station is located at the Cervantes valley floor. The profile shows that the low-resistivity layers are thicker in the valley which is a graben area bounded by the Abra river fault at the west and the east Abra river fault splay to the east. The thickest parts are located near the hot spring locations. Deeper levels are consistently of high resistivity in all the stations covered.

The A-A' profile (Figure 9) shows predominantly low resistivities (< 20 Ωm) with only minor and very thin intercalations of resistivities greater than 50 Ωm to the north at the Namitpit area up to about 400 m depth. At deeper levels, resistivity is in the order of thousands of Ωm. In the south in Cabitin area, high resistivities predominate with some low-resistivity layers (< 50 Ωm). The central area which coincides with the valley is a high resistivity area intercalated with thicker low-resistivity layers. Low-resistivity swells register where hot springs are located. Correlating the resistivity profile with the geological condition of the area, the low-resistivity signature at Namitpit is located within the Malaya River Formation which is composed of dacitic to andesitic volcaniclastics, and intercalated sedimentary sequences characterized by extensive cold hydrothermal alteration of clay and iron hydroxides. Towards the south, from Cervantes to Mankayan, low- resistivity layers seem to thin out.

Profile B-B' (Figure 10) which transects east-west across the cordilleras and the Cervantes and Kagubatan valleys, respectively, shows almost entirely high resistivity values at the cordilleras and the usual high-low resistivity interlayering in the valley. Thin low-resistivity caps occur at the surface of the cordilleras east and west of Cervantes but the resistivity values are close to 50 Ωm compared to resistivity values of < 20 Ωm in the valley.

Profile C-C' (Figure 11) shows thick sections of low resistivity if station V5 and V4 are to be correlated. The low resistivity at station V5 can be explained by its location near the river and Gitlangan hot springs. The low resistivity at V4, however, may be difficult to explain because of insufficient geological information about the area in terms of alteration and structure. It is in station V4 that the level beyond 500 m registered resistivity only in the order of 100 Ωm.

The Schlumberger soundings can be divided into three categories, the first including V6 and V7; the second including V2, V3 and V4; and the third with V1, V5, V8 and V9. In order to detect an anomaly it is necessary to cover an area which also includes undisturbed conditions i.e. in this case an area where

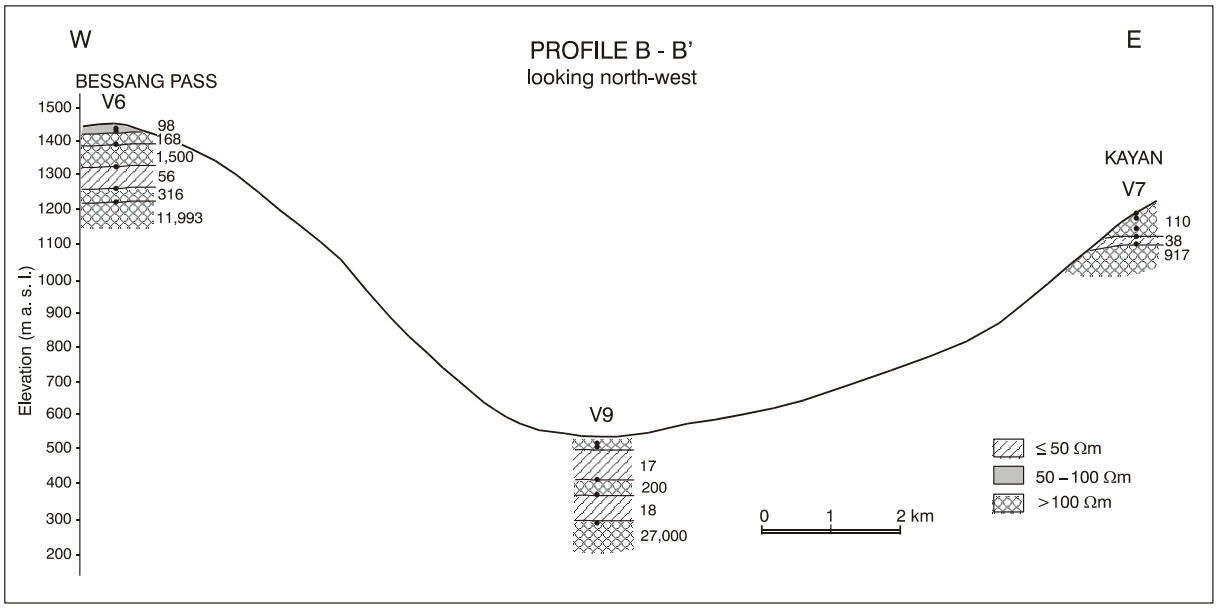

FIGURE 10: Resistivity cross-section B-B'

no geothermal activity is found. Soundings V6 (Bessang Pass), V7 (Kayan) and V4 (Kagubatan) would be expected to be in an area not disturbed by geothermal activity. V6 and V7 show similar features, a thin layer of 30-60 Ωm is impedded in a resistive bedrock (>100 Ωm). V4 at Kagubatan shows quite different features, extremely low resistivities (40 Ωm) to a depth of 350 m with two thin layers of resistivities in the range of 30-60 Ωm.

The soundings V6 and V7 are both within the basement complex (BC on the geological map). The sounding V4, showing very low (<10 Ωm) down to 350 m depth must be within the Balili formation in order to sustain a plausible reason of the low resistivity.

Soundings V2 and V3 show features similar to V4. They show 200-300 m of extremely low resistivity down to 300-400 m depth, with one thin layer of 50-75 Ωm and another of 200 Ωm. They are at the

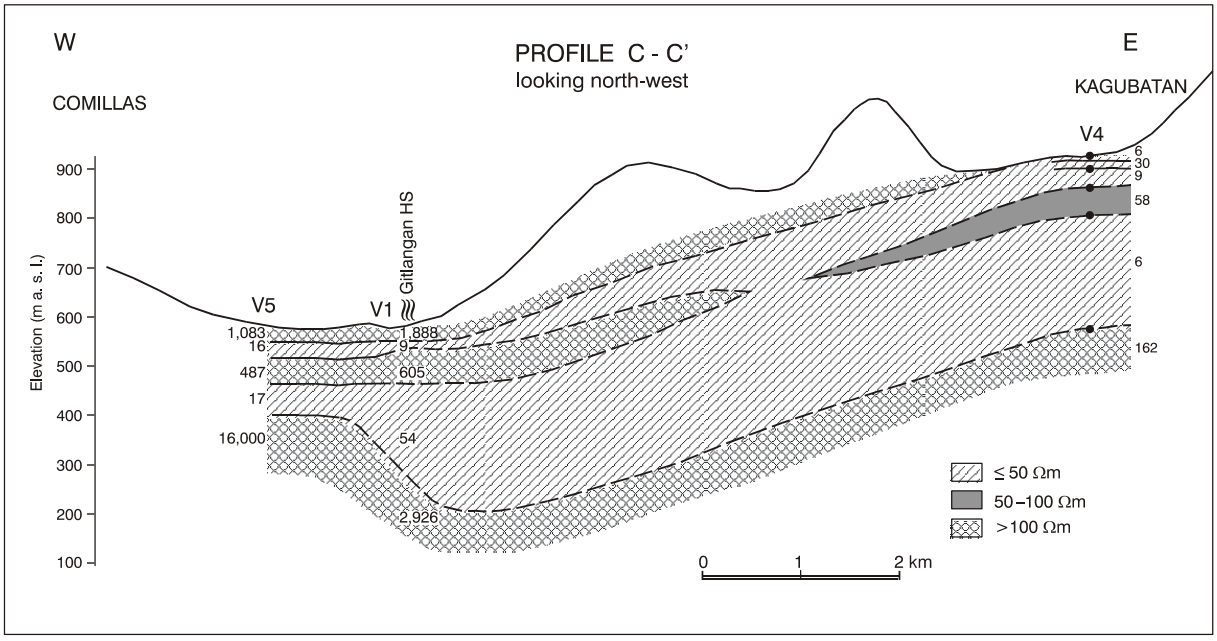

FIGURE 11: Resistivity cross-section C-C'

western margin of the valley, approximately 200 m above the valley floor. They are both within the Malaya River formation. Here again we do not have the geological information to explain the low resistivity. High content of certain clay minerals can cause low resistivity, but we do not know the mineralogy of the MRF formation. Soundings V8, V5, V1 and V9 lie on a profile from Capitin in the south down into the Abra River valley (see profile A-A'). They all have the same character in resistivity distribution; two low-resistivity layers imbedded in resistive surroundings. The upper one has resistivity values in the range of 16-23 Ωm and is very thin (10-20 m) in the south and thickening towards north to approximately 100 m in the valley. The lower layer is 100-200 m thick and has resistivity values in the range of 20-55 Ωm. Those four soundings are all within the same geological formation and the resistivity profile lies close to the geothermal manifestations at Gitlangan, Comillas and Cervantes. It is therefore likely that the resistivity in the two low-resistivity layers is controlled by physical parameters related to geothermal activity. They could in fact be explained as two high-permeability layers containing geothermal water. We have no soundings in the northern part of the Abra River valley but the traverse measurements confirm low resistivity in the valley from Cervantes to Namitpit in the north. There are no soundings in the vicinity of the geothermal springs at Dagnan and Motong.

3.2.3 Conclusions

The most likely conclusion is that the geothermal activity is controlled by the N-S trending faults along Abra river valley. This is confirmed by the geothermal manifestations as well as low-resistivity anomaly in the valley in the transverse measurements. This is also suggested by two low-resistivity layers along a resistivity profile from Capilin down to the Abra valley in the Schlumberger-soundings. Those two low-resistivity layers could be porous layers containing geothermal water.

We have no geological information to explain the low resistivity at Kagubatan and within the Malayan river formation. In order to obtain a model of the geothermal area, more soundings are necessary.

In general, it is quite premature to conclude from the resistivity profiles the factors responsible for the low- resistivity anomalies within the prospect because of insufficient data at hand. The resistivity survey stations are few and located far apart to provide good correlation. The strongly fractured character of the valley and the presence of hot water underneath as evidenced by the presence of the hot springs may, however, explain the low-resistivity anomaly along the southern part of profile A-A'.

4. THE MAGNETOTELLURIC METHOD

4.1 Basic concepts

The magnetotelluric (MT) method employs the fluctuations in the earth s magnetic field which induce electrical currents in the earth. The fluctuations are mainly of two origins. High frequencies (> 1 Hz) occur mainly due to thunderstorms in the equatorial belt, while low frequencies (< 1 Hz) occur mainly due to complex interaction between the solar wind (ionised particles) and the earth's magnetic field. Both the electric and magnetic field components are measured in a magnetotelluric survey.

It has been shown that the electrical field (E) is linearly related to the magnetic field (H) through the impedance tensor (Z) in matrix notation:

$$E = Z \times H \tag{16}$$

or

$$E_x = Z_{xx}H_x + Z_{xy}H_y \qquad \textit{and} \qquad E_y = Z_{yx}H_x + Z_{yy}H_y \tag{17}$$

where E_x, E_y and H_x, H_y are the orthogonal horizontal electrical and magnetic fields, respectively (e.g. Patra and Mallick, 1980).

For a homogenous earth, the resistivity can be calculated from the impedance using the following equation (Patra and Mallick, 1980; Telford et al., 1976):

$$\rho = \frac{1}{\omega\mu}|Z_{xy}|^2 = \frac{1}{\omega\mu}|Z_{yx}|^2 \tag{18}$$

where ρ = Resistivity (Ωm);
ω = Angular frequency, $2\pi f$, with f as frequency (Hz);
μ = Magnetic permeability in (H/m).

Or, in practical units where E is in mV/km and B (= μH) is in gamma or nT, by the equation:

$$\rho \approx 0.2T|Z_{xy}|^2 \approx 0.2T|Z_{yx}|^2 \tag{19}$$

where T = Period in seconds.

If the earth is not homogenous, the resistivity is calculated as if the earth was homogenous and the resulting resistivity is termed as apparent resistivity (ρ_a).

For one-dimensional (1-D) earth where resistivity changes only with depth, the relations of the impedance are as follows (Koefoed, 1994; Hersir and Björnsson, 1991):

$$Z_{xx} = Z_{yy} = 0 \qquad and \qquad Z_{xy} = -Z_{yx} \tag{20}$$

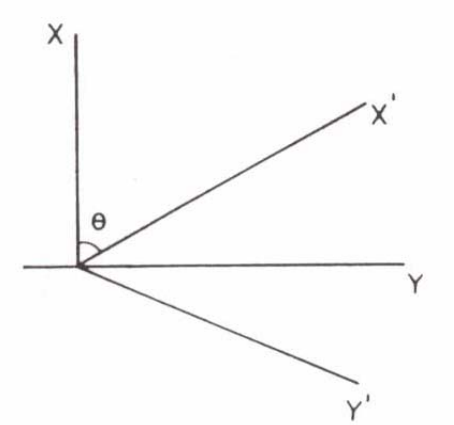

FIGURE 12: Rotation of tensor elements from the measurement axes x-y to the strike of inhomogeneity x' by an angle θ (Patra and Mallick, 1980)

For two-dimensional (2-D) earth where resistivity varies with depth and horizontally in one direction θ (i.e. θ ± 90°), the vector components are rotated from the measurement axes by θ (or θ +90°) such that one of the axes coincides with the strike direction (Figure 12). The rotation angle can be found by minimizing the diagonal elements of the impedance tensor (or alternatively maximizing the off diagonal elements) (Swift, 1967). In the rotated coordinate system, the elements of the impedance tensor (Z') are (Patra and Mallick, 1980):

$$Z'_{xx} = Z'_{yy} = 0 \quad ; \quad Z'_{xy} = \frac{E'_x}{H'_y} = Z_{TE} \quad and$$

$$Z'_{yx} = -\frac{E'_y}{H'_x} = Z_{TM} \tag{21}$$

Z_{TE} is called the E-polarization impedance, where E'_x is parallel the strike (also referred to as the TE mode) and Z_{TM} is called the H-polarization impedance, where E'_y is perpendicular to the strike (also referred to as the TM mode)

For 3-D earth, the relation of the impedance is given as:

$$Z'_{xx} \neq Z'_{yy} \neq 0 \qquad and \qquad Z_{xy} \neq Z_{yx} \tag{22}$$

The 3-dimensionality of the impedance is often described by the *skew* which is calculated by the following equation (Patra and Mallick, 1980):

$$S = \frac{|Z_{xx} + Z_{yy}|}{|Z_{xy} - Z_{yx}|} \quad (23)$$

To facilitate interpretation of 2-D or 3-D earth resistivities by 1-D inversion, an impedance which is invariant for rotation, Z_{det} , is often used and is given by (Zhdanov and Keller, 1994):

$$Z_{det} = (Z_{xx}Z_{yy} - Z_{xy}Z_{yx})^{1/2} \quad (24)$$

This impedance is identical with the true impedance for a horizontally homogenous earth (Zhdanov and Keller, 1994). From this impedance, corresponding apparent resistivities (ρ_{det}) and phases (θ_{det}) are calculated:

$$\rho_{det} = 0.2T|Z_{det}|^2 \quad ; \quad \theta_{det} = arg(Z_{det}) \quad (25)$$

Skin depth is defined as the depth at which the electromagnetic energy is attenuated to 1/e (~ 63 percent). Skin depth can be calculated by the following equation (Patra and Mallick, 1980):

$$\delta = \left(\frac{2}{\omega\mu\sigma}\right)^{\frac{1}{2}} \quad (26)$$

where δ = Skin depth (m);
ω = $2\pi f$ = angular frequency, with f as the frequency (Hz);
μ = Magnetic permeability (H/m);
σ = Conductivity (S/m).

Substituting $\omega = (2\pi / T)$, $\sigma = 1/\rho$ and $\mu = 4\pi \times 10^{-7}$, the equation is reduced to the simple form:

$$\delta = 500\sqrt{\rho T}\ metres \quad or \quad \delta = 0.5\sqrt{\rho T}\ kilometres \quad (27)$$

Thus the skin depth is proportional to the period of oscillation (T), the longer the period, the deeper the depth of penetration. Therefore, low frequencies penetrate deeper into the earth than high frequencies. The attenuation is also dependent on the resistivity; the electromagnetic energy penetrates deeper in highly resistive materials.

4.2 Magnetotelluric interpretation

Magnetotelluric data is obtained by measuring the time series of the electrical and magnetic fields. These time series are transformed into the frequency domain from which the impedance tensor is calculated.

Magnetotelluric interpretation may be done by a 1-D, 2-D or 3-D inversion process but for this exercise, 1-D inversion using the MTTULK program was used to determine the subsurface resistivity structure underneath station #9304 in Central Iceland. The program facilitates both layered and OCCAM 1-D inversion of magnetotelluric data. The OCCAM inversion generates "smooth" varying resistivity models with a minimum structure required by the data (Smith and Booker, 1988).

4.3 Static shifts in magnetotelluric soundings

The static shift is caused by shallow lateral inhomogeneities. Electrical charges build up along the boundaries of the inhomogeneity and distort the apparent resistivity data in such a manner that the apparent resistivity curve is shifted vertically in log space independent of frequency. The static shift does not affect the phase curve. Figure 13 shows the effect of a shallow inhomogeneity to the resistivity structure and the apparent resistivity curve.

The shifts are critical in the interpretation of the magnetotelluric soundings inasmuch as the inverted resistivities are shifted by a factor equal to the amount of the static shift and the inverted depths are also shifted approximately equal to the square root of the static shift (Sternberg et al., 1988). Thus, interpretation of static shifted magnetotelluric data would lead to incorrect results.

For this exercise, transient electromagnetic (TEM) data acquired at the same site as the magnetotelluric measurement was interpreted by 1-D layered and OCCAM inversion using the program TEMINV. The result was used to estimate the static shift in the magnetotelluric data, following the procedure described by Pellerin and Hohmann (1990). The technique is to fix the resistivity and thickness for the shallow layers (from the TEM inversion) and only invert for the deeper layers in the inversion of magnetotelluric data.

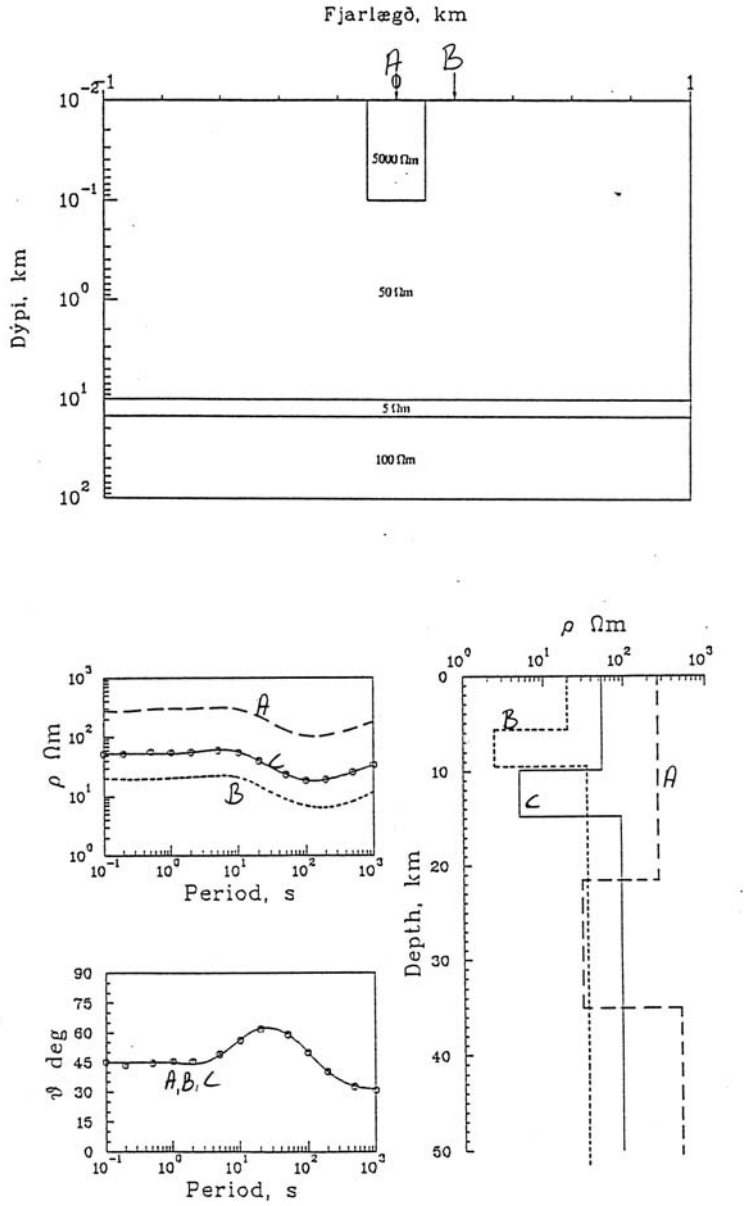

FIGURE 13: MT apparent resistivity curves and structure over a shallow inhomogeneity (A - dashed lines), outside of the inhomogeneity (B - dotted lines), and the calculated best-fit inversion response (C - solid lines), measured MT data are (open circles); note that the phase curve is the same for the resistivity curves A, B, and C (Eysteinsson, 1999)

4.4 Discussion of results

As mentioned in Section 4.2, transient electromagnetic data was acquired at the same site as the magnetotelluric measurement. 1-D inversion of this TEM data using the program TEMINV resolved a three-layer resistivity structure. Both the layered (Figure 14) and OCCAM (Figure 15) models gave similar resistivity structure. From the layered model which best fits the measurements, the resistivities/thicknesses of the three layers are as follows: 30 Ωm/6 m, 120 Ωm/294 m, and 80 Ωm, the last layer being a homogenous half space.

These resistivities and thicknesses, were set as fixed parameters in the initial model prior to inversion of the MT phase data. The phase inversion yielded a calculated apparent resistivity curve which is above the trace of the measured apparent resistivity curve showing a vertical shift of the magnetotelluric data (Figure 16). Therefore, the measured data was shifted by a factor such that the measured apparent resistivity curve fits to the calculated one. The factor used was 1.2.

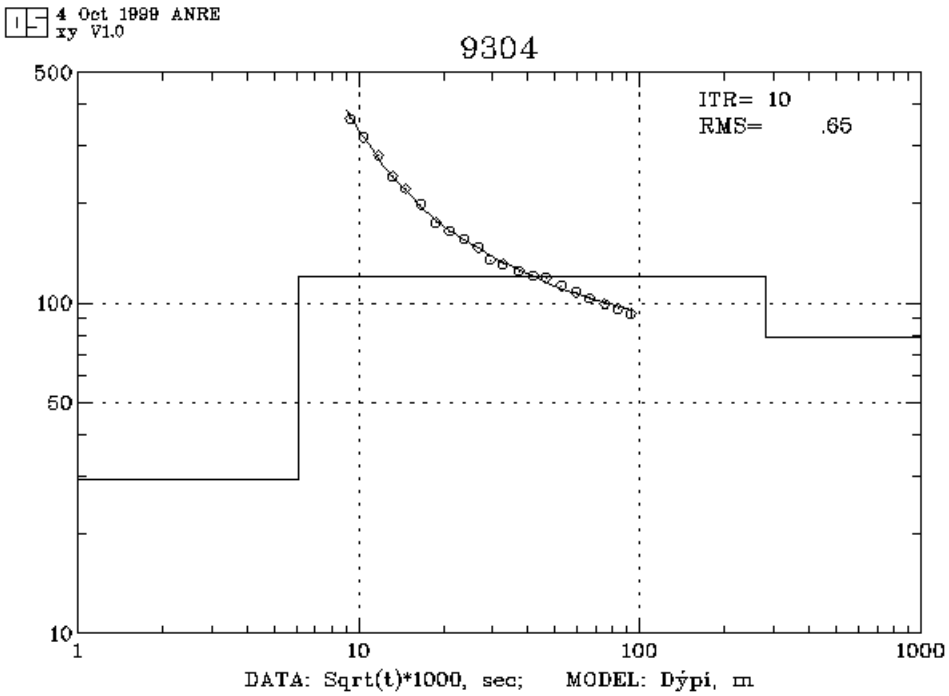

FIGURE 14: TEM 1-D layered model for station 9304

After shifting the apparent resistivity data, an inversion of both the resistivity and the phase was done. The resulting resistivity structure has six layers. The most interesting feature of the model is the low-resistivity layer of 20 Ωm at 21-28 km depth (Figure 17). The OCCAM 1-D inversion of the magnetotelluric data gave similar resistivity structure as the layered model (Figure 18).

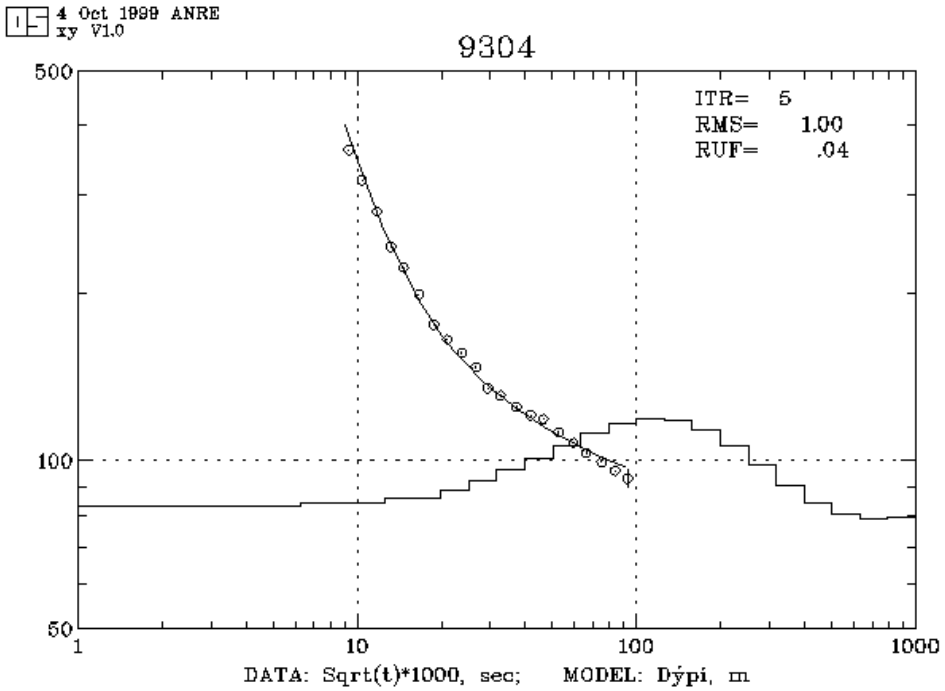

FIGURE 15: TEM 1-D OCCAM model for station 9304

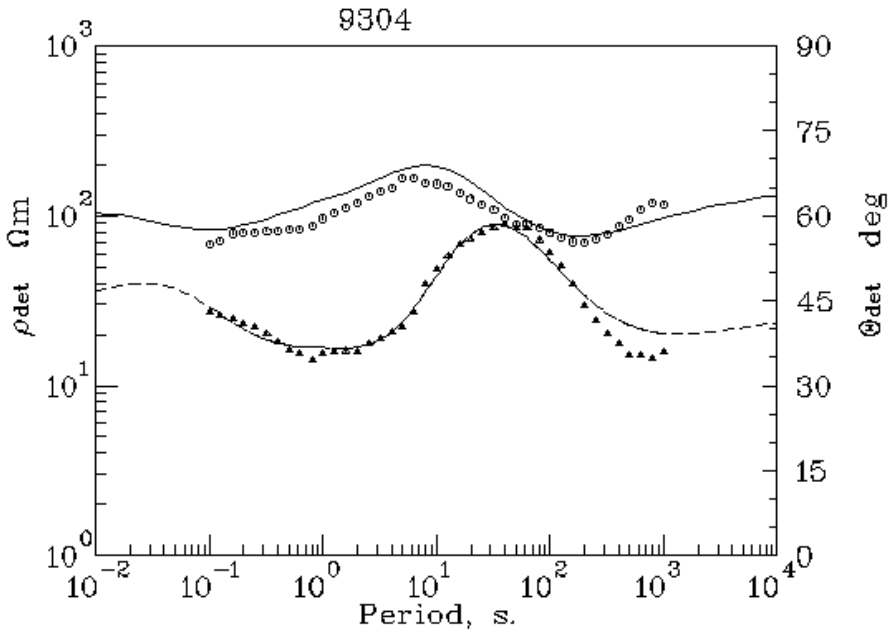

FIGURE 16: Apparent resistivity curve (solid line) calculated from the 1-D layered earth model seen in Figure 17, after the measured apparent resistivity curve (open circles) was shifted; measured curve (triangles) and calculated phase curve (dashed line) also shown

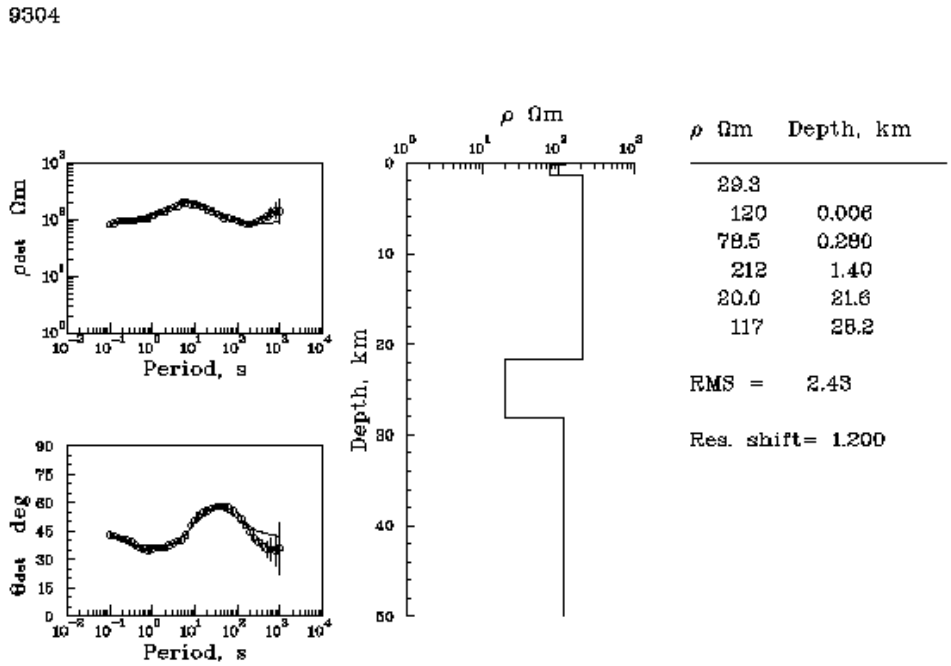

FIGURE 17: Layered resistivity model from magnetotelluric measurements at station 9304

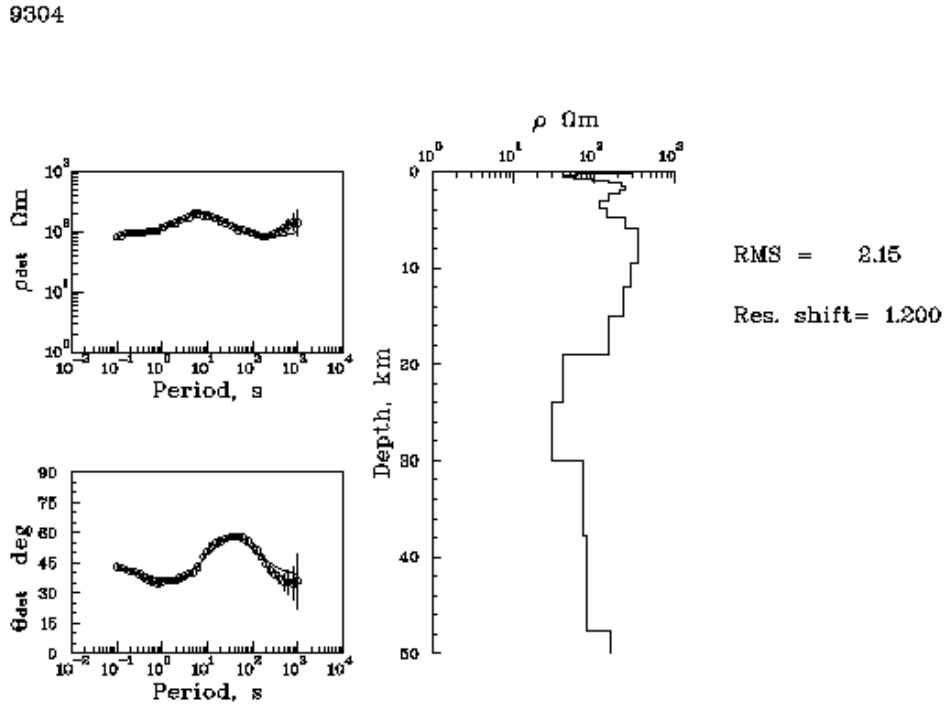

FIGURE 18: OCCAM resistivity model for magnetotelluric measurements at station 9304

5. CONCLUSIONS AND RECOMMENDATIONS

5.1 Schlumberger resistivity

Two low-resistivity anomalies were delineated in the resistivity traverse of the Cervantes geothermal prospect: the Namitpit and Kagubatan anomalies. Based on the profiles constructed from the interpretation of the deeper probing Schlumberger soundings, the general signature is low-resistivity layers occurring within a high-resistivity terrain. The layers swell in the vicinity of the valley especially near the location of the hot springs. The layers thin towards Mankayan, south of the survey area. Extensive low resistivities constitute the upper 400 m of Namitpit and Kagubatan. In all of the sounding stations, high resistivities of the order of thousand Ωm underlie the layered sequence except in the Kagubatan area where the "high" resistivity values measured were close to 100 Ωm.

These findings have to be supported by additional soundings along profiles between current VES stations and, especially, at the Kagubatan area to Mt. Data, where iso-resistivity contours show widening of the low-resistivity anomaly at AB/2 = 500 m towards Mt. Data and where the soundings indicated low-resistivity values at depth compared to other stations. Its continuation within the Lepanto copper mine at Mankayan should also be looked into. It is difficult at this moment to accurately determine the factors responsible for the low-resistivity anomalies due to the limited data to hand, especially within the Kagubatan area. Detailed alteration and structural mapping, therefore, have to be conducted in the area.

5.2 Magnetotelluric sounding

Magnetotelluric sounding can indeed give good resistivity resolution at depth extending to levels of tens of kilometres below the surface, in contrast to the Schlumberger sounding, where depth of penetration is proportional to the current electrode spacing at the surface, and thus, in praxis, the penetration is limited to the uppermost kilometre. The exercise carried out here, also proved the usefulness of complementary TEM data to remove static shift in magnetotelluric soundings caused by surface inhomogeneities.

ACKNOWLEDGEMENTS

I wish to thank the Government of Iceland and the United Nations University Geothermal Training Programme for the opportunity they gave me to widen my knowledge on geothermal exploration, development and utilization. The appreciation also extends to Dr. Ingvar Fridleifsson and Mr. Lúdvík S. Georgsson, UNU Director and Deputy Director, for selecting me as one of this year's trainees; to Dr. Hjalti Franzson who endorsed my participation to the 1999 programme; and to Mrs. Gudrún Bjarnadóttir for the special assistance she provided during my stay in Iceland. My gratitude to my advisers, Hjálmar Eysteinsson and Ragna Karlsdóttir, for guiding me and unselfishly sharing their expertise during the preparation of the project report; and special thanks to all the lecturers for their efforts.

My thanks to the Philippine Department of Energy, especially to Director Griselda J. G. Bausa of the Energy Resource Development Bureau and Mr. Vicente Karunungan, OIC of the Geothermal Division, for allowing me to participate in this course. Special thanks to Mr. Narciso Salvania, former OIC of the Geothermal Division, for endorsing me to the UNU; also to Vanessa Lazaro, our secretary, for handling things for me while I was away. To my family who endured my absence, my love and sincerest appreciation. To God, all glory.

REFERENCES

Árnason, K., 1984: The effect of finite electrode separation on Schlumberger soundings. *54th Annual International SEG Meeting, Atlanta, Expanded Abstracts*, 129-132.

COMEXCO, 1998: *Geoscientific evaluation of the Cervantes geothermal prospect, Cervantes, Ilocos Sur, Philippines.* Department of Energy, Philippines, internal report.

Eysteinsson, H., 1999: *The impedance tensor.* UNU G.T.P., Iceland, unpublished lecture notes.

Hersir, G.P., and Björnsson, A., 1991: *Geophysical exploration for geothermal resources. Principles and application*, UNU G.T.P., Iceland, report 15, 94 pp.

Koefoed, O., 1979: *Geosounding principles, 1: Resistivity sounding measurements.* Elsevier Scientific Publishing Co., Amsterdam, 276 pp.

Patra, H.P. and Mallick, K. 1980: *Geosounding principles 2. Time-varying geoelectric soundings*. Elsevier Scientific Publishing Co., Amsterdam, 419 pp.

Pellerin, L., and Hohmann, G.W., 1990: Transient electromagnetic inversion: A remedy for magnetotelluric static shifts. *Geophysics, 55-9,* 1242-1250.

Smith, J.T., and Booker J.R., 1988: Magnetotelluric inversion for minimum structure. *Geophysics,53-12,* 1565-1576.

Sternberg, B.K., Washburn, J.C., and Pellerin, L., 1988: Correction for the static shift in magnetotellurics using transient electromagnetic soundings. *Geophysics, 53-11,* 1459-1468.

Swift Jr., C.M., 1967: *A magnetotelluric investigation of an electrical conductivity anomaly in the southwestern United Staes.* Ph.D. thesis, Massachusetts Institute of Technology, MA, USA.

Telford, W.M., Geldart, L.P., Sheriff, R.E., and Keys, D.A., 1976: *Applied Geophysics.* Cambridge University Press, Cambridge, 860 pp.

Zhdanov, M.S., and Keller G.V., 1994: *The geoelectrical methods in geophysical exploration.* Elsevier Scientific Publishing Co., The Netherlands, 873 pp.

APPENDIX 1: Resistivity models for the Schlumberger resistivity soundings from Cervantes geothermal prospect, Cervantes, Ilocos Sur, Philippines

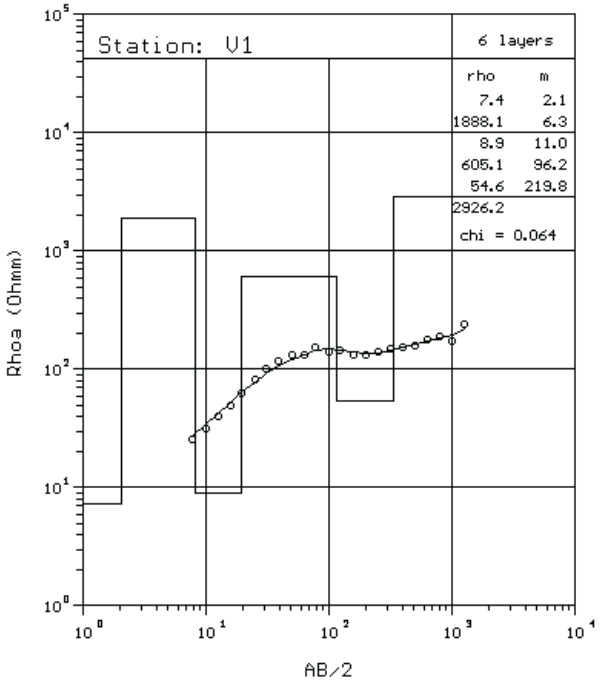

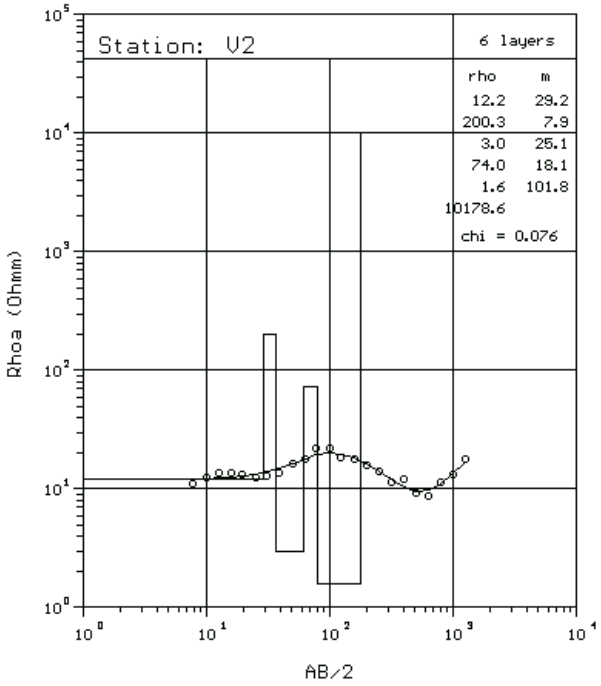

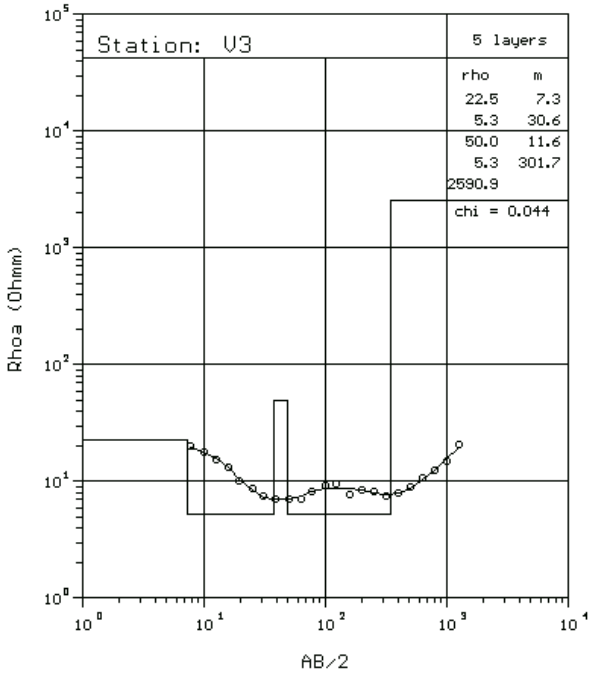

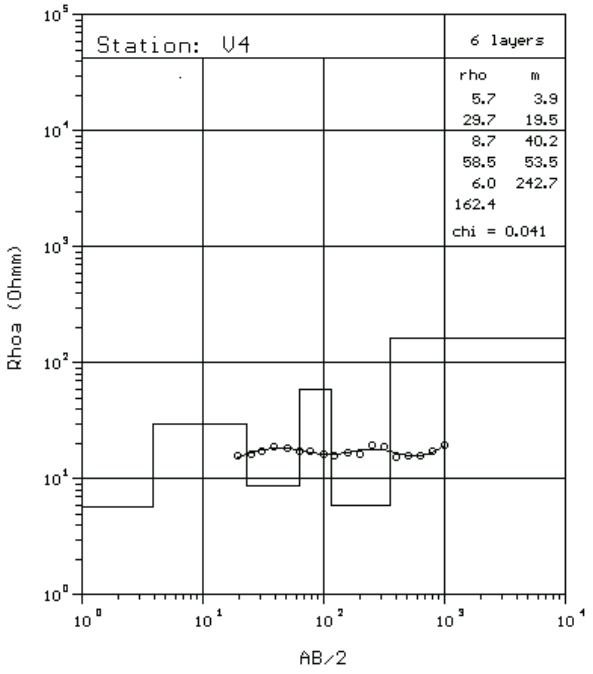

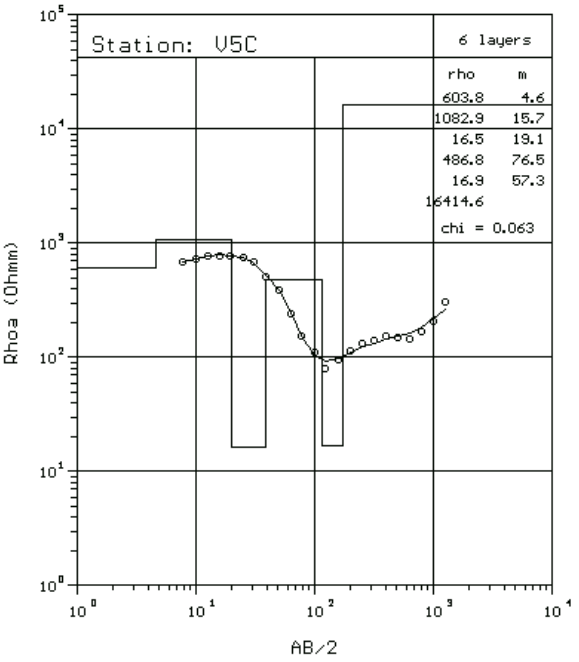
Station: V5C
6 layers
rho m
603.8 4.6
1082.9 15.7
16.5 19.1
486.8 76.5
16.9 57.3
16414.6
chi = 0.063
Rhoa (Ohmm)
AB/2

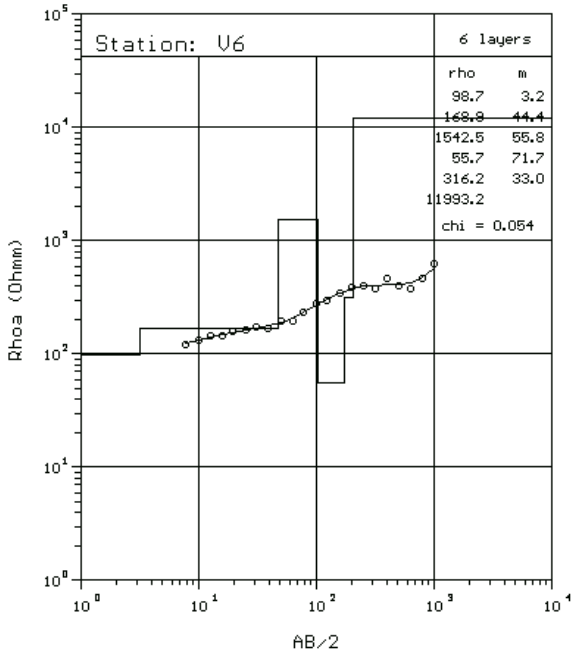
Station: V6
6 layers
rho m
98.7 3.2
168.8 44.4
1542.5 55.8
55.7 71.7
316.2 33.0
11993.2
chi = 0.054
Rhoa (Ohmm)
AB/2

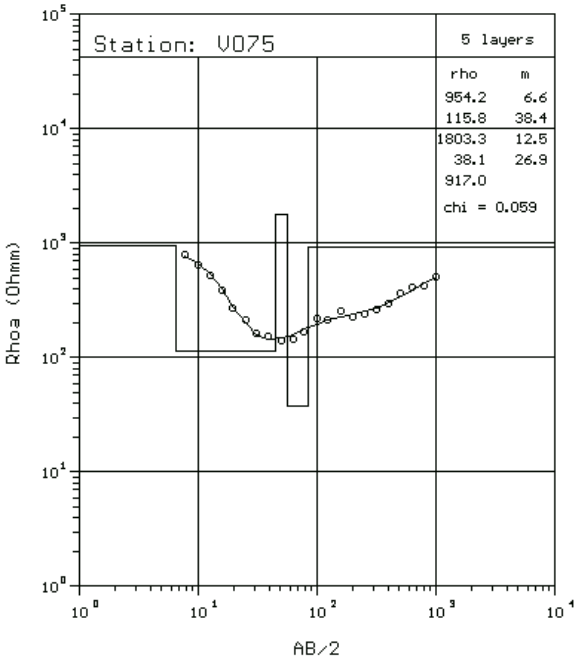
Station: V075
5 layers
rho m
954.2 6.6
115.8 38.4
1803.3 12.5
38.1 26.9
917.0
chi = 0.059
Rhoa (Ohmm)
AB/2

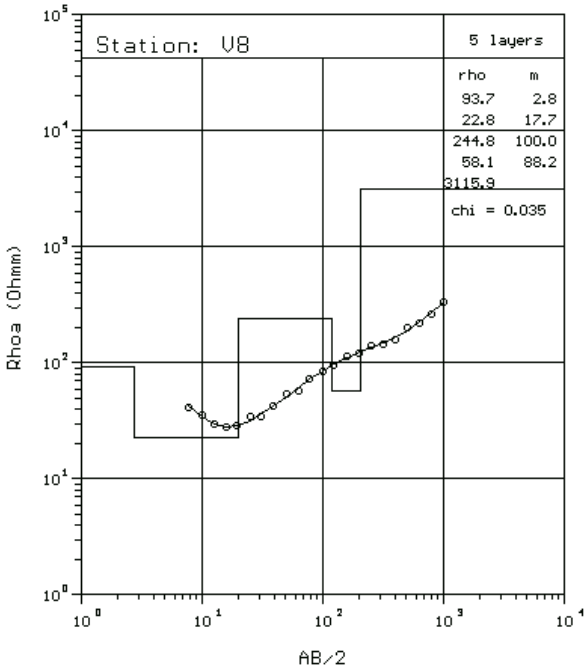
Station: V8
5 layers
rho m
93.7 2.8
22.8 17.7
244.8 100.0
58.1 88.2
3115.9
chi = 0.035
Rhoa (Ohmm)
AB/2

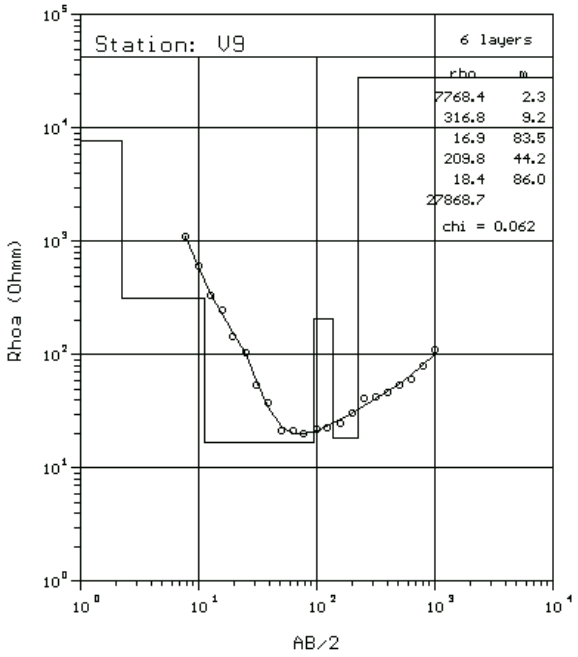

APPENDIX 2: Measured apparent resistivity (open circles) and phase curve (squares) for magnetotelluric station 9304 with plot of measured TEM data (crosses) at the same site